

The Effects of North Atlantic SST and Sea Ice Anomalies on the Winter Circulation in CCM3. Part I: Main Features and Storm Track Characteristics of the Response

GUDRUN MAGNUSDOTTIR

Department of Earth System Science, University of California, Irvine, Irvine, California

CLARA DESER AND R. SARAVANAN

National Center for Atmospheric Research, Boulder, Colorado*

(Manuscript received 16 January 2003, in final form 6 October 2003)

ABSTRACT

Observed multidecadal trends in extratropical atmospheric flow, such as the positive trend in the North Atlantic Oscillation (NAO) index, may be attributable to a number of causes. This study addresses the question of whether the atmospheric trends may be caused by observed trends in oceanic boundary forcing. Experiments were carried out using the NCAR atmospheric general circulation model with specified sea surface temperature (SST) and sea ice anomalies confined to the North Atlantic sector. The spatial pattern of the anomalous forcing was chosen to be realistic in that it corresponds to the recent 40-yr trend in SST and sea ice, but the anomaly amplitude was exaggerated in order to make the response statistically more robust. The wintertime response to both types of forcing resembles the NAO to first order. Even for an exaggerated amplitude, the atmospheric response to the SST anomaly is quite weak compared to the observed positive trend in the NAO, but has the same sign, indicative of a weak positive feedback. The anomalies in sea ice extent are more efficient than SST anomalies at exciting an atmospheric response comparable in amplitude to the observed NAO trend. However, this atmospheric response has the opposite sign to the observed trend, indicative of a significant negative feedback associated with the sea ice forcing. Additional experiments using SST anomalies with opposite sign to the observed trend indicate that there are significant nonlinearities associated with the atmospheric response.

The transient eddy response to the observed SST trend is consistent with the positive NAO response, with the North Atlantic storm track amplifying downstream and developing a more pronounced meridional tilt. In contrast, the storm track response to the observed sea ice trend corresponds to a weaker, southward-shifted, more zonal storm track, which is consistent with the negative NAO response.

1. Introduction

Trends in climate variables have been the subject of intense study in recent years. Of particular importance is the question of whether the observed trends are attributable to natural variability or to anthropogenic forcing effects. Since the climate system is composed of many interacting components, such as the atmosphere and the ocean, a trend in one component could well be caused by trends in another component. For example, the observed trend in atmospheric flow could be forced by trends in oceanic surface conditions. Understanding the interactions between different components of the

climate system would greatly help us in interpreting the observed climatic trends.

In this study, we focus on one particular form of interaction, that between the atmosphere and the ocean, in the North Atlantic region. The North Atlantic Oscillation (NAO) is the dominant mode of atmospheric low-frequency variability over the North Atlantic and adjacent continents during the winter season (e.g., Hurrell 1995). It is characterized by a seesaw in mass between the subpolar low and the subtropical high. A positive NAO index refers to exaggerated pressure extrema in these two semipermanent systems. A negative NAO index refers to the reverse situation. On interannual and shorter time scales the NAO is thought to be primarily driven by internal atmospheric variability (Saravanan 1998). On longer time scales it is probably forced, at least in part, by other components of the climate system such as the ocean and sea ice. Changes in the NAO go hand in hand with changes in the atmospheric distribution of temperature, precipitation, storminess, and other features of the atmospheric circulation (e.g., Hur-

* The National Center for Atmospheric Research is sponsored by the National Science Foundation.

Corresponding author address: Dr. Gudrun Magnusdottir, Department of Earth System Science, University of California, Irvine, Irvine, CA 92697-3100.
E-mail: gudrun@uci.edu

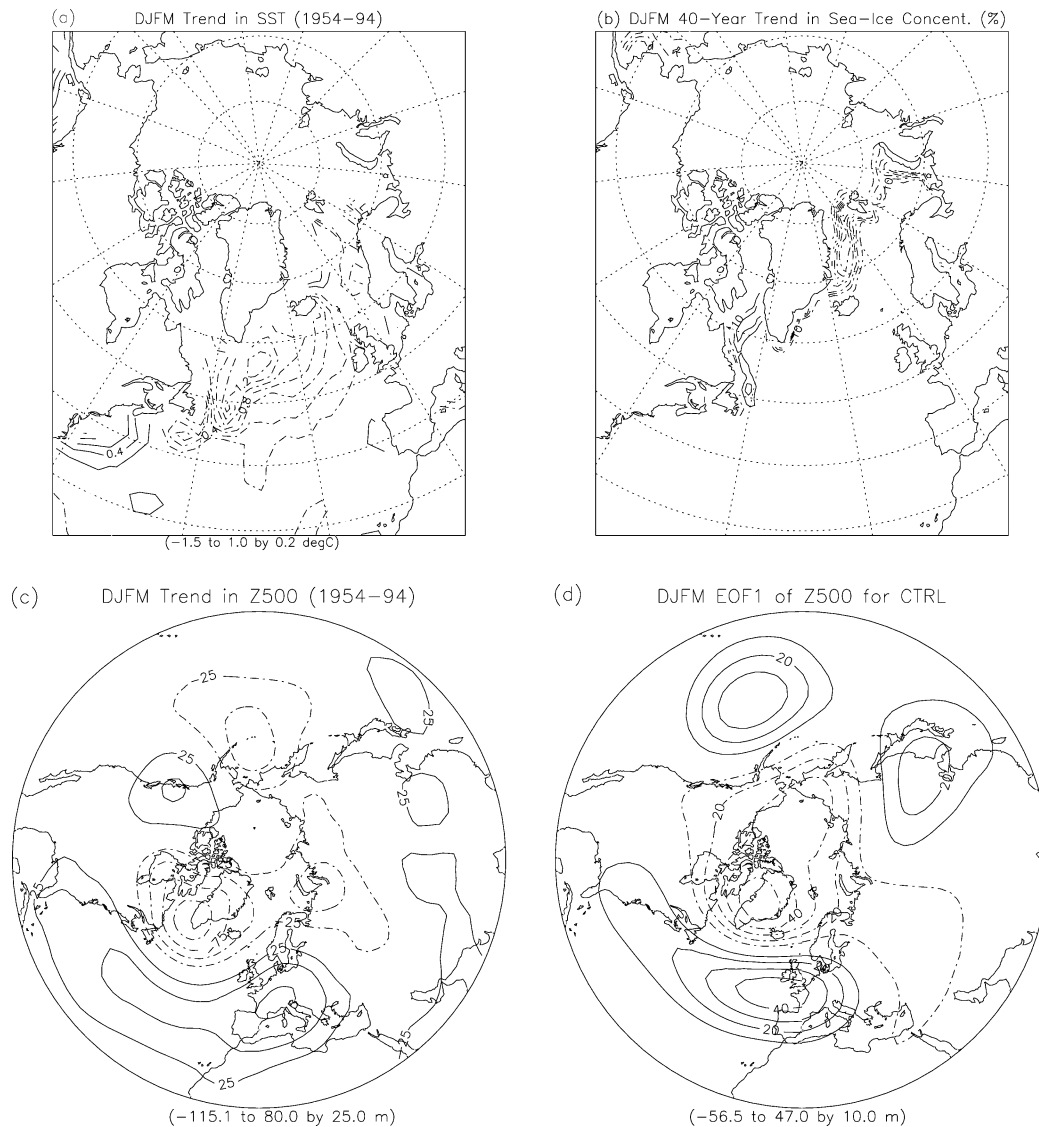


FIG. 1. (a), (b), (c) The 40-yr trends in winter-mean (DJFM) SST, sea ice concentration, and 500-hPa geopotential height, respectively. Positive contours are solid, negative contours are dashed-dotted, and the zero contour is suppressed. Note that the projection in (a), (b) is polar stereographic but the figures only include the Arctic Ocean and North Atlantic Ocean north of 30°N . In (a), the least squares trend in SST is for the period 1954–94. Contour interval is 0.2 K. In (b), the trend in sea ice concentration is for the period 1958–97 in $\% (40 \text{ yr})^{-1}$. Contour interval is 10%. In (c), the least squares trend in 500-hPa geopotential height is for 1954–94. Contour interval is 25 m. Panel (d) shows the first EOF of the DJFM-mean 500-hPa geopotential height field in the control simulation. Contour interval is 10 m.

rell and van Loon 1997). Stephenson and Pavan (2003) recently investigated the NAO and its variability in 17 coupled climate models and compared the results to the observational record. To avoid getting embroiled in semantics let us clarify terminology. We shall use the term NAO for the Arctic Oscillation (AO) as well as the NAO. The area of influence of the AO is the entire polar cap, whereas the NAO is limited to the North Atlantic and surrounding coastal areas. Some studies suggest that there are fundamental differences between the two terms (e.g., Ambaum et al. 2001), while others argue that they are simply different characterizations of the same phe-

nomenon (e.g., Wallace 2000). Here, we use the term NAO even though the area considered may be the entire polar cap.

We consider the observed linear trend over a recent 40-yr period in three different climatic variables: the 500-hPa geopotential height, sea surface temperatures (SSTs), and sea ice concentration (Figs. 1a–1c). For the 500-hPa height and SST, the linear trends were computed by least squares fitting of a straight line to boreal winter (December–March) means of the climatic variables from 1954 to 1994. The geopotential height data were obtained from the National Centers for Environ-

mental Prediction–National Center for Atmospheric Research (NCEP–NCAR) reanalysis (Kalnay et al. 1996), the SST data from version 2 of the Global Sea Ice and Sea Surface Temperature (GISST2) dataset (Rayner et al. 1995). The sea ice concentration trend is for the period 1958–97, and is taken from Deser et al. (2000). The trend in winter-mean, sea ice concentration is a drastic reduction in sea ice east of Greenland over the 40-yr period, and a lesser increase west of Greenland and into the Labrador Sea. The SST trend has an extensive area of cooling in the subpolar gyre that is of maximum amplitude 1.5 K, a lesser warming off the east coast and a lesser yet warming in the far northeastern Atlantic. Note that the 500-hPa height trend pattern (Fig. 1c) has a significant projection onto the NAO spatial pattern, consistent with the decadal trends toward a more positive NAO noted by Hurrell (1995). For comparison, in Fig. 1d we show the first EOF of the winter-mean 500-hPa geopotential height for a control simulation in our atmospheric general circulation model (AGCM) where SST and sea ice extent have a climatological annual cycle that is repeated every year. Note the similarity of the spatial patterns in Figs. 1c and 1d, especially over the North Atlantic and adjacent continents.

After inspecting Fig. 1, one may pose the question: Were the trends in the SST and sea ice caused by the observed trends in atmospheric flow, or were the trends in the atmospheric flow caused by the trends in SST and sea ice? Atmospheric forcing of the ocean tends to dominate air–sea interaction in the mid- and high latitudes (Deser and Timlin 1997; Frankignoul et al. 1998; Saravanan 1998). Therefore, to a first approximation, one may expect that the SST and sea ice trends are just a response to the atmospheric trends. Indeed, Seager et al. (2000) and Deser et al. (2000) invoke atmospheric forcing to explain the observed variability in SST and sea ice, respectively. However, there is still the possibility that there is a significant feedback associated with the atmospheric response to the oceanic trends, although this may not be the dominant form of interaction. In particular, we would like to know if the atmospheric response to the oceanic trends has the same spatial pattern as the observed atmospheric trend. If that were the case, it would be indicative of a positive feedback in the climate system. The results of Rodwell et al. (1999) and Peng et al. (2002) would seem to suggest that there is a weak positive feedback. However, there are significant subtropical and tropical components to the SST anomalies used in these studies, making it difficult to determine if the feedback is truly extratropical. If the atmospheric response had the opposite sign to the observed trend, it would be indicative of a negative feedback. In contrast to the above two studies, a recent study by Schneider et al. (2003) finds little resemblance between the observed atmospheric trend over the North Atlantic and the simulated ensemble mean of North Atlantic atmospheric response in experiments forced by

the observed trend in global SSTs. In the present study and a companion study (Deser et al. 2004, hereafter referred to as Part II), we analyze a series of AGCM experiments that examine the winter response to observed trends in lower boundary conditions in the extratropical North Atlantic. We consider the response to both SST anomalies and sea ice anomalies.

The atmospheric response to extratropical SST anomalies has been the subject of numerous observational and modeling studies. However, this response is still poorly understood, largely due to the large internal variability of the midlatitude atmosphere, which tends to obscure any direct effect of the SST anomaly. Kushnir et al. (2002) summarized observational and modeling studies of the atmospheric response to isolated midlatitude SST anomalies. The response of AGCMs to interannual SST anomalies is weak, but not negligible, and sometimes nonlinear to the amplitude and sign of change. The response may also be nonlinear in terms of geographical regions, such that the effects of isolated SST anomalies in different regions may not be additive. Several modeling studies have found that the response is highly sensitive to the location of the SST anomaly relative to the storm track and the mean jet, as well as to the jet strength. This result is rather worrisome in light of the fact that some of the models have significant errors in the location and strength of these features. Thus, results tend to be model dependent. The AGCM that we use, version 3 of the Community Climate Model (CCM3), has been found to produce realistic simulations of the extratropical mean winter circulation and its variability (e.g., Hurrell et al. 1998; Saravanan 1998; Magnusdottir 2001).

The effect of sea ice anomalies on the atmospheric flow has received less attention than the effect of midlatitude SST anomalies. Many earlier studies used idealized sea ice perturbations, such as removing all of the sea ice or changing its extent or concentration in a zonally symmetric manner, to force the atmosphere (e.g., Simmonds and Budd 1991; Murray and Simmonds 1995; Menendez et al. 1999). Some recent studies have begun using sea ice perturbations derived from observed anomaly patterns to force the atmosphere. Honda et al. (1999) used sea ice anomalies based upon observed extreme conditions of heavy and light sea ice cover in the Sea of Okhotsk, with some exaggeration of the spatial extent of the anomaly. Alexander et al. (2004) used actual observed sea ice anomalies, for specific seasons that had large anomalies, to force an AGCM.

What sets the current experiments apart from many other AGCM studies is the realistic spatial structure of the boundary forcing, and the parallel investigation of the relative roles of SST and sea ice forcing. The spatial structure of the SST and sea ice anomalies is based on that of the recent 40-yr trends (Figs. 1a,b), restricted to the North Atlantic (NA) region only. We investigate the response with respect to amplitude and polarity of the SST forcing. For each polarity of SST forcing, we con-

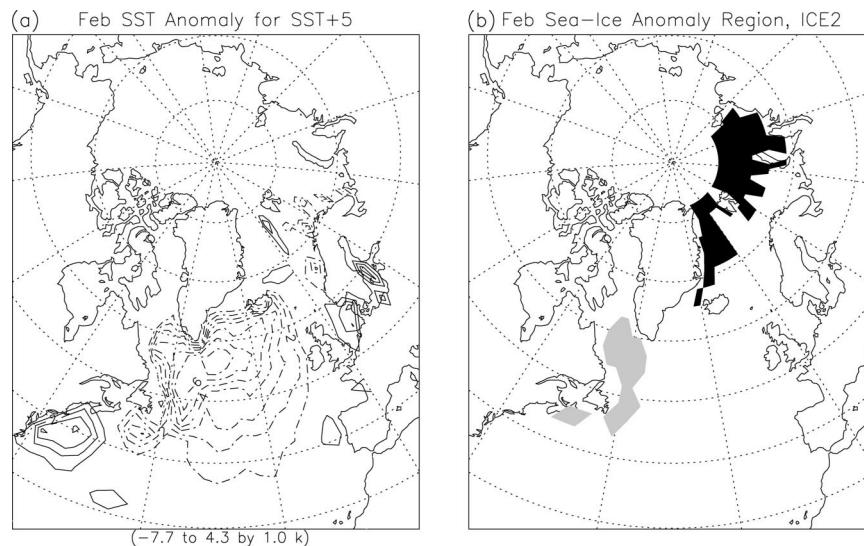


FIG. 2. (a) SST anomaly for the month of Feb for the case SST+5 (corresponding to bicentennial SST trend). Contour interval is 1 K, positive contours are solid, negative contours are dashed-dotted, the zero contour is suppressed. (b) Sea ice anomaly for the month of Feb for the case ICE2. Light shading indicates that sea ice is added, dark shading indicates that sea ice is removed. The projection is the same as in Figs. 1a,b.

sider two amplitudes, corresponding to centennially and bicentennially scaled trends. We examine two amplitudes of sea ice forcing and we separately examine the two major regions of the exaggerated amplitude, sea ice forcing. The amplitude of sea ice forcing is harder to quantify than that of SST forcing since the model assumes that either there is sea ice or there is open ocean at a given grid point. Therefore, we only consider the trend in the extent of sea ice, not in its concentration, even though the trend in concentration is expected to play an important role. The exaggerated sea ice anomaly corresponds to approximately double the areal extent of the trend in sea ice change over a recent 40-yr period.

When the SST is changed, the sea ice is held fixed at the climatological extent. Conversely, when we force the model by changing the sea ice distribution, we hold SST fixed at the climatological value. We have used exaggerated forcing amplitudes because the atmospheric response to midlatitude SST and sea ice anomalies is relatively weak, that is, when compared to the amplitudes of internally generated atmospheric variability. The forcing amplitudes that we have used allow us to obtain a statistically robust response with about 60 yr of model integration.

The outline of this study is as follows: section 2 gives an overview of the model and the numerical experiments. Section 3 examines the midtropospheric response, both in terms of winter-mean and monthly mean geopotential height. Section 4 contains a more thorough examination of results for the December–January–February–March (DJFM) mean response in various fields including surface energy flux, precipitation, the lower-level temperature, the upper-level flow, and the storm

track response as seen in time-filtered (co)variance fields. Finally, section 5 contains some concluding remarks.

A companion study (Part II) uses an EOF decomposition technique to provide a detailed analysis of the response in terms of a directly forced component versus a component produced by the projection of the response on the internal variability of the model.

2. Model and experiments

The numerical model is the NCAR CCM3 in the standard configuration as detailed in Kiehl et al. (1998). The model resolution is T42 with 18 vertical layers in a hybrid-sigma coordinate system. This version of CCM3 presents major improvements over earlier versions especially in terms of the physical parameterizations resulting in a more realistic thermal structure and hydrologic cycle. Hack et al. (1998) present a comprehensive study of the simulated hydrologic and thermodynamic characteristics of CCM3 based on a 15-yr integration using observed monthly mean SSTs from 1979 to 1993. Hurrell et al. (1998) use the same 15-yr simulation to examine the representation of the dynamical fields by CCM3. This simulation is almost identical to our control case, CTRL, which is an 84-yr simulation using 1 yr of climatological monthly mean SSTs that are repeated each year. The instantaneous dynamical fields are saved twice per day. Additional fields are saved as daily and monthly averages. Magnusdottir (2001) analyzed the representation of Northern Hemispheric (NH) storm tracks in the control simulation as compared to NCEP reanalysis. They found that compared to other AGCMs,

TABLE 1. The different numerical experiments and the imposed oceanic boundary conditions in SST and in sea ice. SST_{clim} refers to the climatological SST, NA_{trend} refers to the 40-yr trend in SST in the extratropical North Atlantic. $SICE_{\text{clim}}$ refers to the climatological sea ice extent in the North Atlantic and Arctic Ocean. Here E_{trend} and W_{trend} refer to the 40-yr trend in sea ice extent, east and west of Greenland, respectively. The max response in 500-hPa geopotential height (m) in each case is shown in the last column.

Experiment name	Monthly SST	Monthly sea ice extent	Max 500-hPa (m) geopotential response
CTRL	SST_{clim}	$SICE_{\text{clim}}$	0
SST+2.5	$SST_{\text{clim}} + 2.5 \times NA_{\text{trend}}$	$SICE_{\text{clim}}$	-21
SST+5	$SST_{\text{clim}} + 5 \times NA_{\text{trend}}$	$SICE_{\text{clim}}$	-30
SST-2.5	$SST_{\text{clim}} - 2.5 \times NA_{\text{trend}}$	$SICE_{\text{clim}}$	42
SST-5	$SST_{\text{clim}} - 5 \times NA_{\text{trend}}$	$SICE_{\text{clim}}$	82
ICE1	SST_{clim}	$SICE_{\text{clim}} + W_{\text{trend}} + E_{\text{trend}}$	52
ICE2	SST_{clim}	$SICE_{\text{clim}} + 2 \times (W_{\text{trend}} + E_{\text{trend}})$	91
ICELAB	SST_{clim}	$SICE_{\text{clim}} + 2 \times W_{\text{trend}}$	-39
ICEGRN	SST_{clim}	$SICE_{\text{clim}} + 2 \times E_{\text{trend}}$	106

the North Atlantic storm track is quite well represented in CCM3. Its strength (in terms of high-pass-filtered transient eddy streamfunction variance) is slightly underestimated and its shape tends to be slightly too zonal over the mid- to eastern North Atlantic.

The prescribed lower boundary condition is determined from monthly mean SST fields, linearly interpolated in time between months. Sea ice is prescribed in the model whenever the SST goes below the threshold value of -1.8°C . Since sea ice is not explicitly represented in the model, only surface properties such as albedo and the surface energy fluxes change when the sea surface is covered by ice. We use two different boundary forcings, that of SST anomalies and that of sea ice anomalies. When forcing the model with SST anomalies, we hold the sea ice extent constant at climatological values. When forcing with sea ice anomalies, we hold the SST distribution constant at climatological values. The anomalies are calculated for each calendar month. For most of the year the boundary-forcing anomalies in each case are quite similar. Thus, we only show these fields for one month, that of February.

Figure 2a shows the spatial structure of the SST perturbation that is added to the SST for February. This structure is based on the least squares linear trend in the GISST2 dataset for the same month (Rayner et al. 1995), but only for the years from 1954 to 1994. (The entire dataset extends from 1903 to 1994). The trend was computed for the NA region, north of 20°N , and the SST anomaly corresponds to the pattern of the trend (scaled by a factor of 5 in Fig. 2a) north of 30°N . The SST anomaly was set to zero at 20°N and constrained to vary linearly between 20° and 30°N . The familiar structure of the North Atlantic tripole of SST variability (e.g., Kushnir et al. 2002, and references therein) is evident from the figure. As displayed in the figure, the trend is scaled to correspond to an equivalent bicentennial trend in SST. The different experiments vary in terms of the amplitude of the perturbation, not its spatial structure. The term ‘‘trend factor’’ is used to refer to the factor by which the 40-yr trend in SST is multiplied

in each experiment before adding it to the SST field. We conducted five different experiments, characterized by trend factors 0, 2.5, -2.5 , 5, and -5 , which we name CTRL, SST+2.5, SST-2.5, SST+5, and SST-5, respectively. We shall primarily discuss results from the two SST-forced cases: SST-5 and SST+5.

We conducted four experiments where the sea ice extent was changed, but the SST was held fixed at climatological values. As in the case for SST forcing, we considered an exaggerated anomaly, that was based on the 40-yr monthly trend in sea ice distribution in the North Atlantic/Arctic region from Deser et al. (2000), but the areal extent of the anomaly was approximately doubled. Figure 2b shows the February sea ice anomaly for this exaggerated case that we term ICE2. The dark shaded area indicates removal of sea ice, the light shaded area indicates that sea ice is added. The anomaly has decreased sea ice east of Greenland and increased sea ice west of Greenland and into the Labrador Sea. We ran an experiment that we term ICE1 that has about half the areal extent of the sea ice anomaly of ICE2 and corresponds more closely with the 40-yr trend. We ran two additional experiments, one where we only applied the sea ice forcing of ICE2 west of Greenland (increased ice extent in Fig. 2b), termed ICELAB, and the other where we only applied the forcing east of Greenland (removed sea ice), termed ICEGRN. We shall primarily focus attention on the case ICE2.

All experiments were run for at least 61 yr. The experiments CTRL and SST+5 are two decades longer. Table 1 summarizes all nine experiments. The 40-yr SST trend is denoted by NA_{trend} , the sea ice trend east of Greenland is denoted by E_{trend} , and that west of Greenland is denoted by W_{trend} . For both sets of experiments, the boundary forcing for February, which is shown in Fig. 2, is a good representation of the forcing applied over the entire winter season. The last column in Table 1 shows the maximum (or minimum for negative numbers) response in 500-hPa geopotential height in each case. The value of this number gives a good indication of the robustness of the response in many other fields. This is further discussed in the next section.

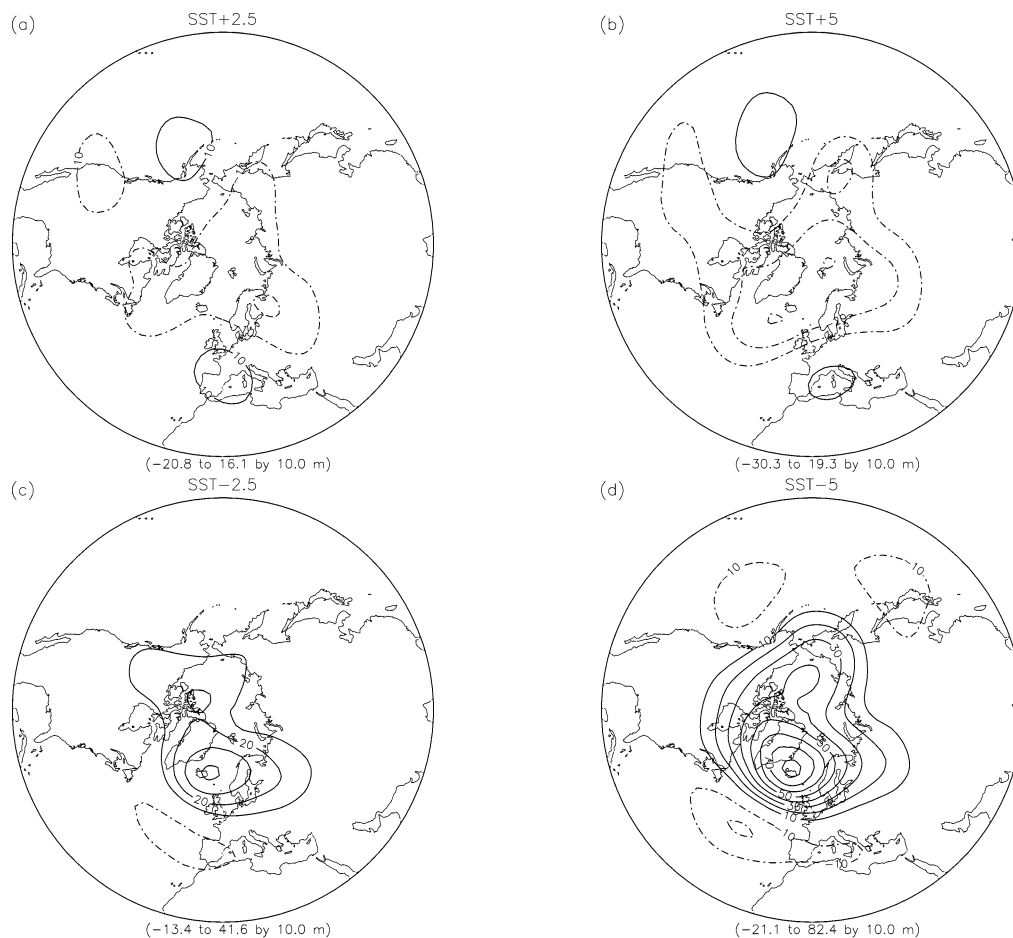


FIG. 3. DJFM-mean response in 500-hPa geopotential height for (a) SST+2.5, (b) SST+5, (c) SST-2.5, (d) SST-5, (e) ICE1, (f) ICE2, (g) ICELAB, and (h) ICEGRN. Contour interval is 10 m. Positive contours are solid, negative contours are dashed-dotted, and the zero contour is suppressed.

3. The large-scale midtropospheric response

The response in any field is obtained by subtracting the mean of the field in the control from the mean of the field in the perturbation experiment. We take the winter season to include December–March. This choice for the extent of the winter season was guided in part by the first EOF of 500-hPa height for the control case, in this instance computed only over the NA basin (where the boundary forcing is applied). It clearly corresponds to the NAO for those four months, whereas for November and April that was not the case.

The response in geopotential height is equivalent barotropic in the free atmosphere. The winter-mean response in 500-hPa geopotential is shown in Figs. 3a–h for all cases. The response is statistically significant at 95% according to a t test roughly for absolute values greater than 10 m (not shown). Overall, the pattern of response is reminiscent of the first EOF of geopotential height in CTRL (Fig. 1d), at least over the polar cap and farther south in the North Atlantic and adjacent continents. For the SST experiments (Figs. 3a–d) a far

stronger (and opposite) response is obtained when we subtract the anomaly in Fig. 2a, which corresponds to a positive SST anomaly in the subpolar gyre, than when we add it to the climatological SST field. Thus the response is nonlinear in the polarity of the SST anomaly. The response in the two former cases (SST-2.5 and SST-5) corresponds to positive height anomalies over the polar cap with negative anomalies farther south in the North Atlantic. For this polarity of the SST forcing, where we subtract the SST trend (Figs. 3c,d), the response appears quite linear in amplitude of forcing. That is not the case for the experiments where the trend is added as can be seen from Figs. 3a,b and from the last column of Table 1, which gives the greatest amplitude of the response in each case. To briefly summarize: the experiments that are forced by SST anomalies that are in the same sense as the trend in SST (Figs. 3a,b), show a 500-hPa geopotential height response that is of similar spatial pattern to that of the trend in 500-hPa geopotential shown in Fig. 1c, but of smaller amplitude. This occurs even though the amplitude of the

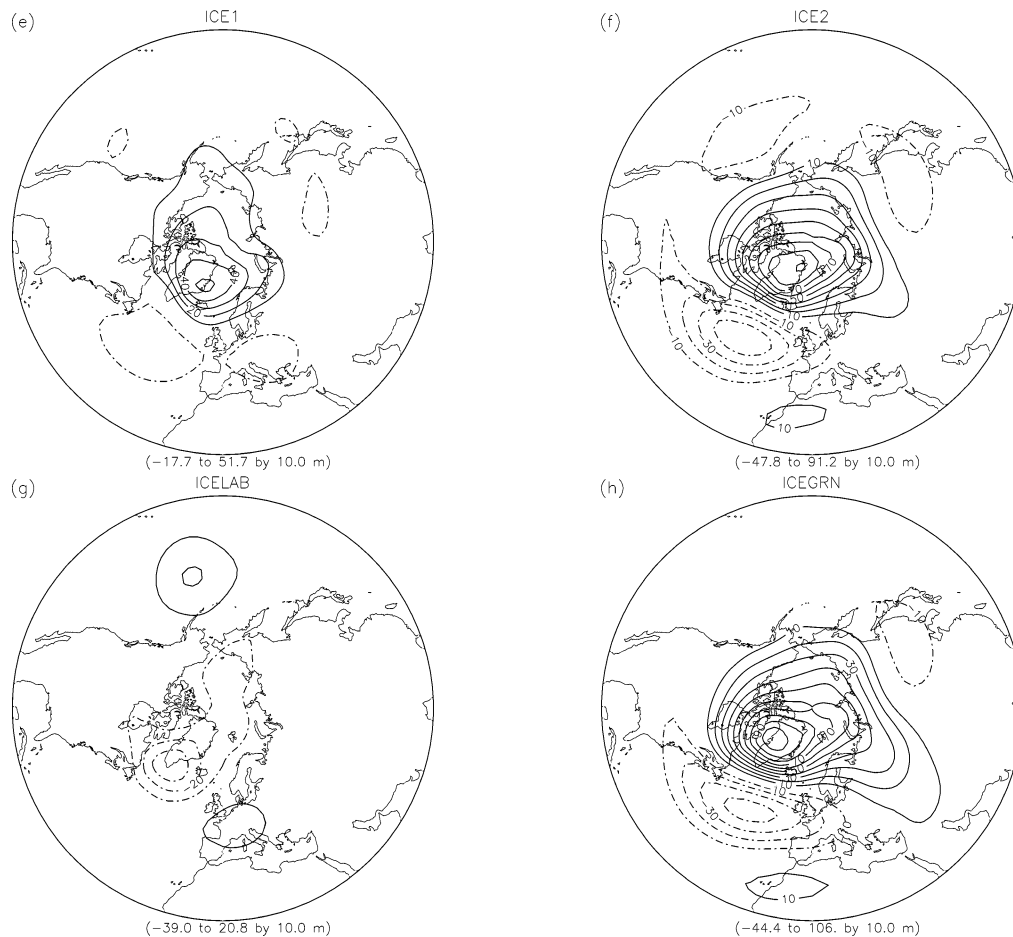


FIG. 3. (Continued)

SST anomaly pattern has been amplified fivefold in experiment SST+5 (Fig. 3b). This is indicative of a relatively weak positive feedback, consistent with results of Rodwell et al. (1999) and Peng et al. (2002).

For the two sea ice experiments, ICE1 and ICE2 (Figs. 3e,f), the sign of the response is opposite to that of the positive trend-factor SST cases, or positive over the polar cap and negative farther south. The amplitude of response in ICE2 is considerably greater than for SST+5, but still somewhat smaller than the trend in 500-hPa geopotential height (Fig. 1c). This indicates a negative feedback. We did not perform experiments with combined SST and sea ice forcing in the initial set of experiments, but based on the strength of the sea ice forced response compared to that forced by the SST trend one might conclude that the overall feedback is negative. Later we found that this is indeed the case. However, it can be dangerous to assume any type of linearity. For example, it is striking how similar the response of ICEGRN (Fig. 3h), where the forcing is confined to sea ice removal east of Greenland, is to the full, exaggerated forcing, sea ice experiment (ICE2), which in addition to the above includes an area of in-

creased sea ice southwest of Greenland. By contrast, the response in experiment ICELAB (Fig. 3g) does not have the same spatial pattern and is of considerably smaller amplitude and opposite sign. In fact, for ICELAB only the region of negative response over the southern tip of Greenland and surrounding ocean is statistically significant at 95% according to a local t test. The response in other experiments was substantially more robust according to this test.

We want to explore further the similarity of the general pattern of response of the 500-hPa geopotential to the first EOF of the DJFM-mean 500-hPa height in CTRL. This EOF (Fig. 1d), which corresponds to the NAO, explains 32% of the variance. The second EOF corresponds to the Pacific–North American (PNA) pattern and explains 13% of the variance. The domain for the EOF calculation was the Northern Hemisphere, north of 30°N. We ask if there is a substantial shift of an NAO index in the three large forcing-amplitude experiments (SST+5, SST−5, and ICE2). Since the polarity of the EOF in Fig. 1d corresponds to a positive NAO, we simply project the response time series in each case onto this pattern to obtain the shift in NAO index.

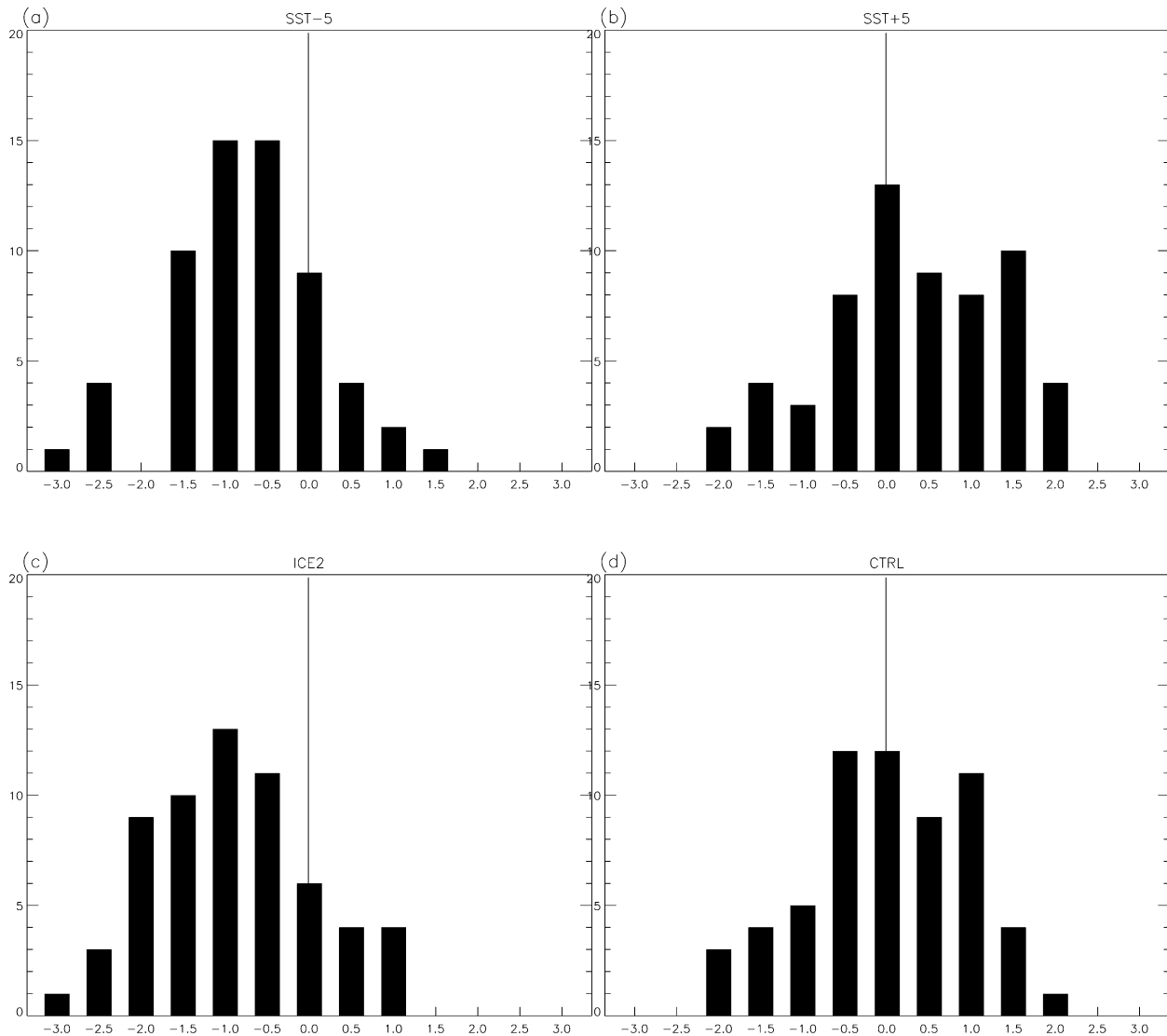


FIG. 4. Histograms resulting from the projection of the time series of DJFM-mean response in 500-hPa geopotential height in each case onto the first EOF of the DJFM-mean 500-hPa geopotential height in the control case (CTRL). The horizontal axis is labeled in std devs, the vertical axis indicates number of samples (winters). The vertical line indicates zero std dev. For consistency between different cases, only the first 61 yr of each time series was used. (a) Case SST-5. The mean is shifted to -0.8σ . (b) Case SST+5. The mean is shifted to $+0.31\sigma$. (c) Case ICE2. The mean is shifted to -0.9σ . (d) Control case for comparison. The mean is at 0.028σ .

In Fig. 4 we plot the histograms of the resulting projected time series for the four cases: SST-5 in (a), SST+5 in (b), ICE2 in (c), and CTRL in (d), for comparison. (In this instance, we only use the first 61 yr of each time series for consistency between cases.) The vertical dashed-dotted line in the plots indicates zero standard deviation (σ), and as expected the mean of CTRL is zero. For SST-5 in (a) the mean is shifted to -0.8σ , for ICE2 in (c) it is shifted to -0.9σ . The shift for the mean of SST+5 is much less or $+0.31\sigma$. Thus, in both experiments, SST-5 and ICE2, the shift of the NAO index is almost of a standard deviation to negative values whereas in experiment SST+5 the shift is only a third of that, and to a positive value. Note that this

methodology assumes that the NAO in all the experiments maintains the same spatial structure and same variance as CTRL. It assumes that only the mean may shift.

The month to month variability in 500-hPa geopotential response was quite pronounced in the different cases, especially between the months of February and March. In Fig. 5 we show this monthly response for the four winter months for the SST-5 case. The largest response is reached at the end of winter in March (Fig. 5d). The largest 500-hPa geopotential response was also reached in March in the ICE2 experiment. In contrast, the SST+5 experiment showed the largest geopotential response in February and the smallest response in March.

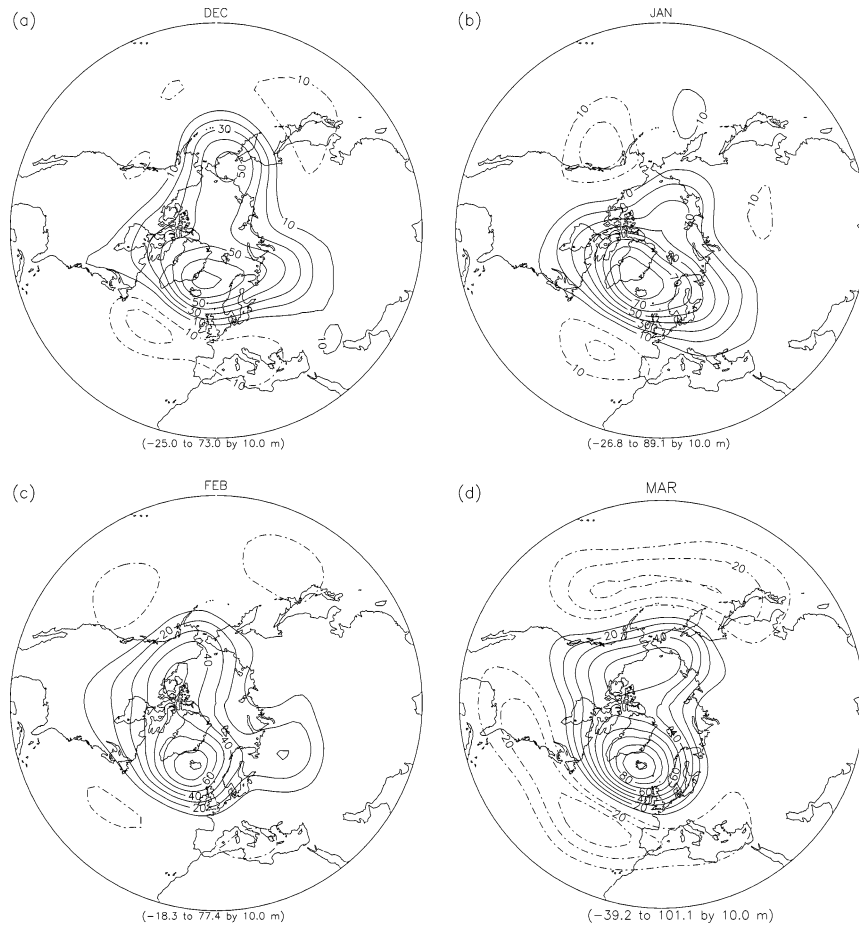


FIG. 5. Monthly mean response in 500-hPa geopotential height for SST-5: (a) Dec, (b) Jan, (c) Feb, (d) Mar. Contour interval is 10 m, positive contours are solid, negative contours are dashed-dotted, and the zero contour is suppressed.

4. The mean winter response

Here we examine further the winter-mean response. First we consider the local response in surface energy flux, precipitation as well as the thermal and geopotential response in vertical cross sections along a fixed latitude. We then examine the upper-tropospheric response. Of particular interest is how the storm track responds in relation to the midtropospheric, mass-field response, and how transient eddy feedback may be modifying the response in each case.

a. The local response

The response in net surface energy flux (radiative, latent, and sensible) is shown in Figs. 6a,b,c for cases SST-5, SST+5 and ICE2, respectively. For comparison, Fig. 6d shows the net surface energy flux for CTRL. The response in the experiments forced by SST anomalies show the familiar negative feedback in surface flux (Barsugli and Battisti 1998), such that the response to warm SST anomalies is increased net flux into the atmosphere, and decreased surface flux for negative SST

anomalies. Note that the response in these two experiments is not equal and opposite. The surface response to positive SST anomalies is stronger, however the spatial pattern is quite similar. The spatial pattern of the response is also similar for the two cases that have SST anomalies corresponding to the centennial positive and negative SST trend (SST+2.5 and SST-2.5, not shown), but the amplitude is not simply half that of the corresponding bicentennial case, rather it is smaller.

A different sea ice distribution corresponds to isolating the atmosphere from the ocean where sea ice is extended into regions where it was previously absent, and opening the ocean surface to the atmosphere in regions that were previously covered with ice. As shown in Fig. 6c, this results in a much more drastic response in surface flux (note that the contour interval in Fig. 6c is double that in Figs. 6a,b). Where ice is removed, east of Greenland, the surface flux has a large positive response, followed by a negative response downstream. Where sea ice is extended into the Labrador Sea, the response in surface flux is strongly negative, followed by a positive response downstream. The fact that the

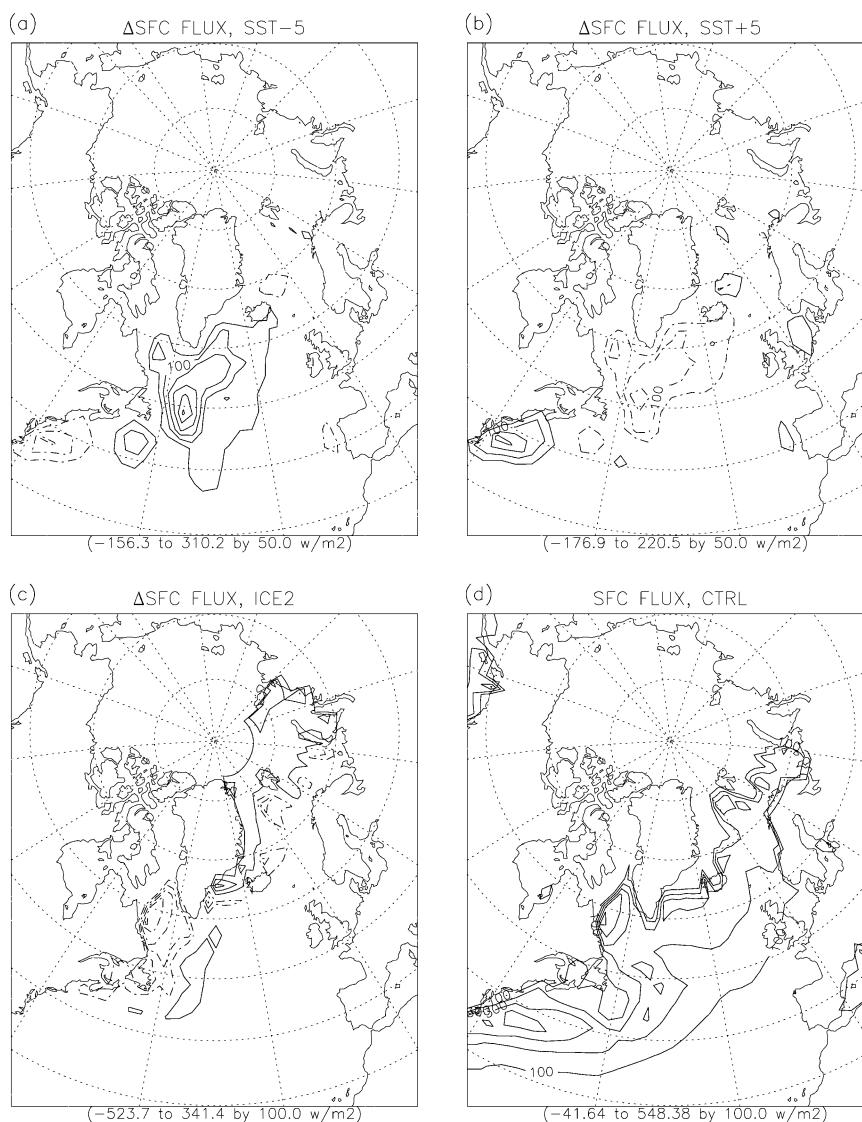


FIG. 6. DJFM-mean response in net surface energy flux (the projection is the same as in Figs. 1a,b): (a) SST-5, (b) SST+5, (c) ICE2. Contour interval is 50 W m^{-2} in (a), (b); and 100 W m^{-2} in (c); negative contours are dashed-dotted; and the zero contour is suppressed. (d) Net DJFM-mean surface energy flux in the CTRL simulation. Contour interval is 100 W m^{-2} .

response in surface energy flux is strongly positive downstream of where the sea ice has been extended reflects the impact of isolating the atmosphere from the ocean over the ice, such that it becomes cold and dry, and when it gets advected over the open ocean there is a sudden burst in surface energy flux. The opposite applies downstream of areas that have been cleared of sea ice. In the case ICELAB (not shown), the response in surface fluxes was almost identical to the part of the response in ICE that is south of 63°N .

Let us consider a longitudinal cross section through 57°N , crossing the NA basin from 70°W to 30°E . This latitude circle crosses through the center of the most intense SST anomaly as seen in Fig. 2a. In Fig. 7, we

show the response in geopotential and temperature for SST-5 (Figs. 7a,c) and SST+5 (Figs. 7b,d) in the longitude-height plane. The response in geopotential (Figs. 7a,b) clearly shows the equivalent barotropic nature of the response, reaching maximum amplitude at tropopause level, above the maximum SST anomaly. The warming in SST-5 (Fig. 7c) decreases with height in the troposphere. Above the tropopause the response in temperature is negative in this case. For SST+5 (Fig. 7d) the cooling at the surface decreases with height and changes to warming in the stratosphere. This difference in the temperature response leads to very different vertical development in the two cases. When the atmosphere is warmed from below (as in SST-5), static

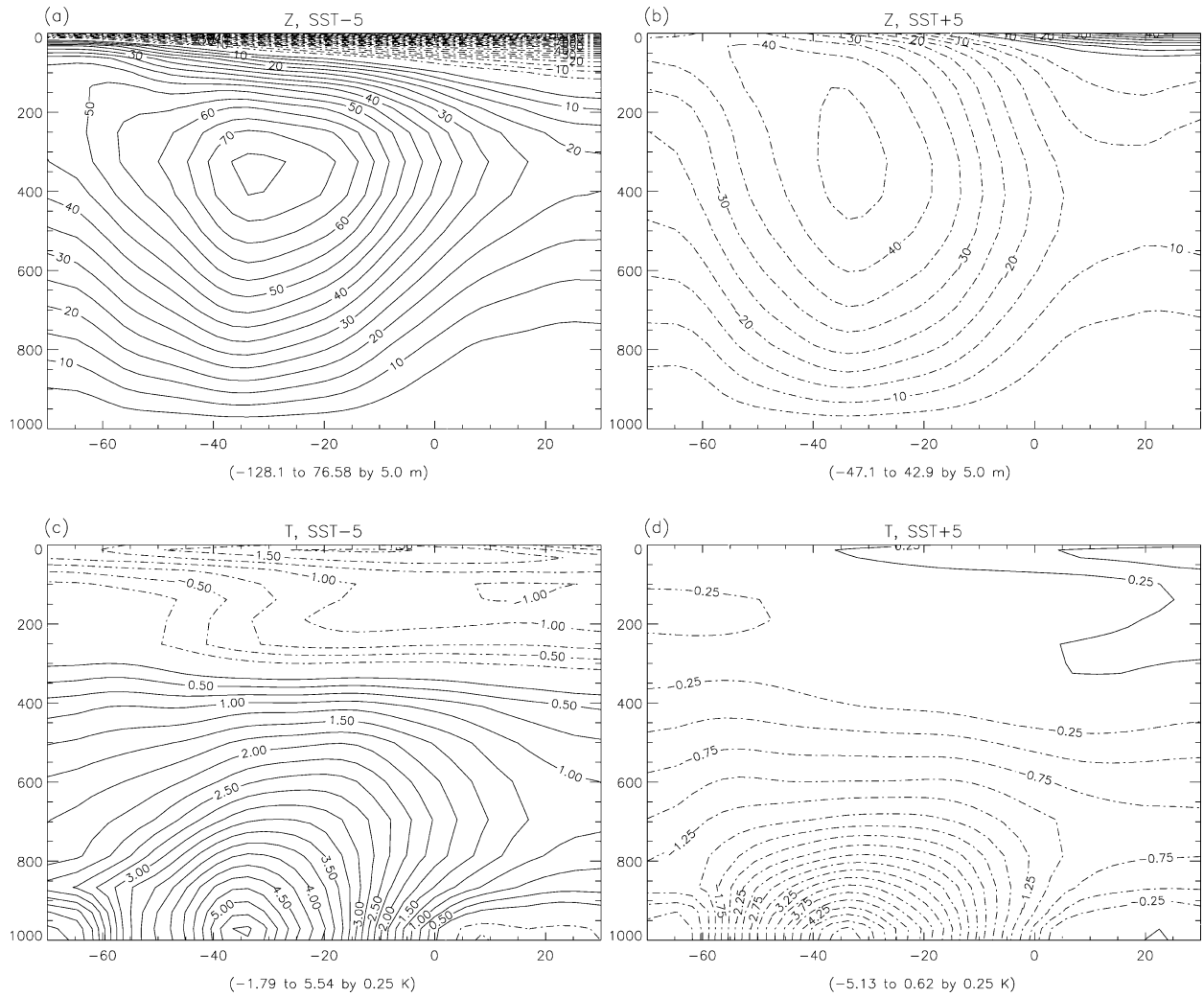


FIG. 7. Cross sections through the longitude–height plane at 57°N, extending from 70°W to 30°E, showing the DJFM response of (a), (c) SST–5 and (b), (d) SST+5. Negative contours are dashed–dotted. Response in geopotential is shown in (a), (b); contour interval is 5 m. Response in temperature is shown in (c), (d); contour interval is 0.25 K.

stability is decreased leading to more vertical development, whereas with the cooling from below (SST+5), static stability is increased. This effect shows up clearly in cross sections for heating rate (not shown) where the atmospheric response of positive heating rate extends almost to tropopause level, whereas the response of cooling has less vertical extent. This will be discussed further in Part II of this study.

As might be expected, there is close correspondence in each case between the response in total precipitation, the vertically integrated total heating, and convective cloudiness. The first is shown in Fig. 8. There is increased precipitation over the warm SST anomalies, decreased precipitation over the cold SST anomalies, with amplitudes of the former greater than those of the latter, for each anomaly pattern with both polarities. This may be explained partly by the nonlinear dependence of saturation vapor pressure on temperature. Vertical stability

plays a more important role as discussed above. Downstream of the major NA SST anomaly, there is a smaller SST anomaly of opposite sign in the region of the North Sea (see Fig. 2a). The response in precipitation in this area shows up clearly, and surprisingly, the signal is even stronger when this SST anomaly is negative in sign (as it is in SST–5). (The stronger response in SST–5 in this area can also be seen in cross sections for heating rate.) This may indicate nonlocal control on the precipitation in the area since positive SST anomalies generate a larger local response in precipitation than negative SST anomalies. In fact, in the next section we shall see that SST+5 and SST–5 respond oppositely in storm track activity in this area.

The ICE2 case shows a strong positive precipitation response where sea ice has been removed, east of Greenland. Immediately downstream of this area, precipitation has decreased. Precipitation is also strongly reduced

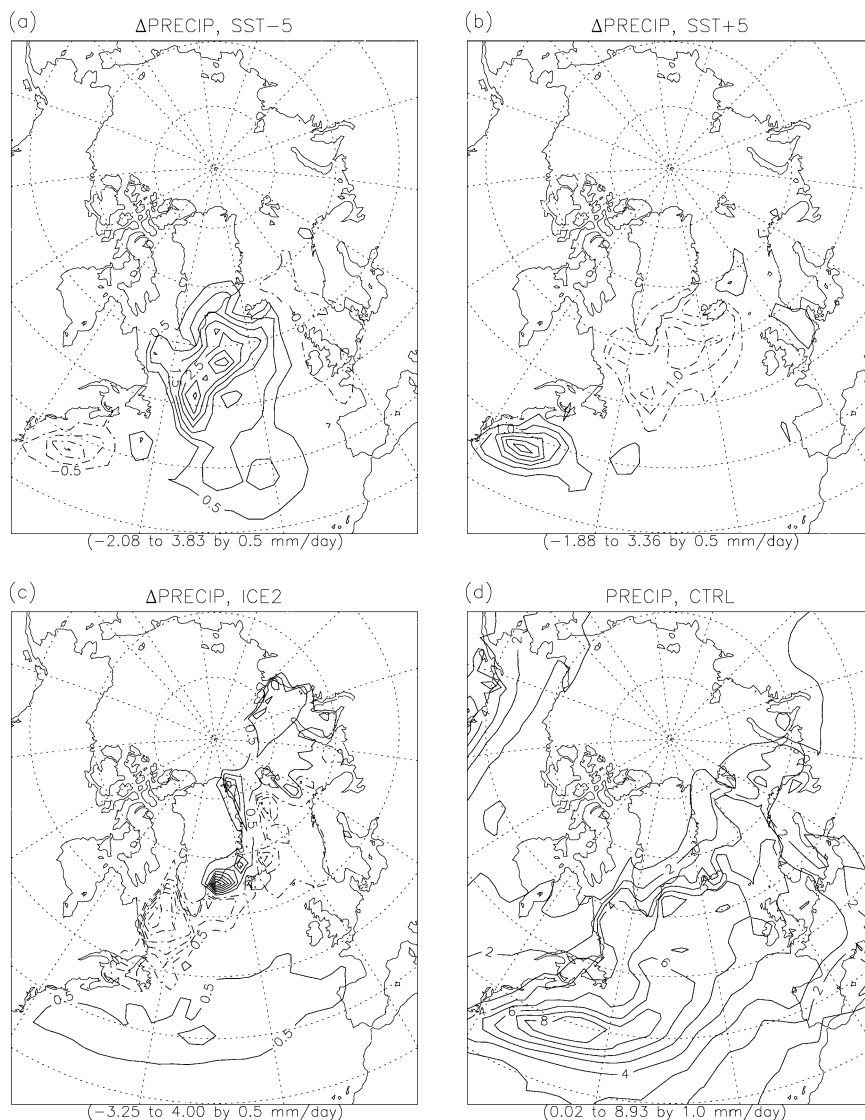


FIG. 8. DJF-mean response in precipitation (the projection is the same as in Figs. 1a,b): (a) SST-5, (b) SST+5, and (c) ICE2. Contour interval is 0.5 mm day⁻¹, negative contours are dashed-dotted, and the zero contour is suppressed. (d) Net DJF-mean precipitation in the CTRL simulation. Contour interval is 1 mm day⁻¹.

over the area where sea ice has been extended. We examined cross sections (not shown) of the response in geopotential, temperature and heating rate, in this case through 71°N, which is through the most extensive area of sea ice removal within the NA basin. These cross sections revealed that in spite of the large response in surface flux, the heating was quite shallow, or confined to the layer below 600 hPa. We attribute this vertical structure to the large static stability that has to be overcome at this high latitude (see Part II of this study for details).

Finally, there is a broad area of weakly increased precipitation over most of the Atlantic between 35° and 50°N in the ICE2 case. This increased precipitation in

midlatitudes, along with the response in 500-hPa geopotential, is reminiscent of a negative NAO scenario. We shall examine this further in the next section, in terms of the storm track response.

b. The free tropospheric response

We shall focus on the mean upper-tropospheric response in terms of streamfunction, depicted by $\bar{\psi}$, and derived or closely related fields. First, let us comment briefly on data analysis and notation. We use square brackets to represent a zonal average, the star to represent the deviation from the zonal average (e.g., $x = [x] + x^*$). The overbar represents a time mean over the

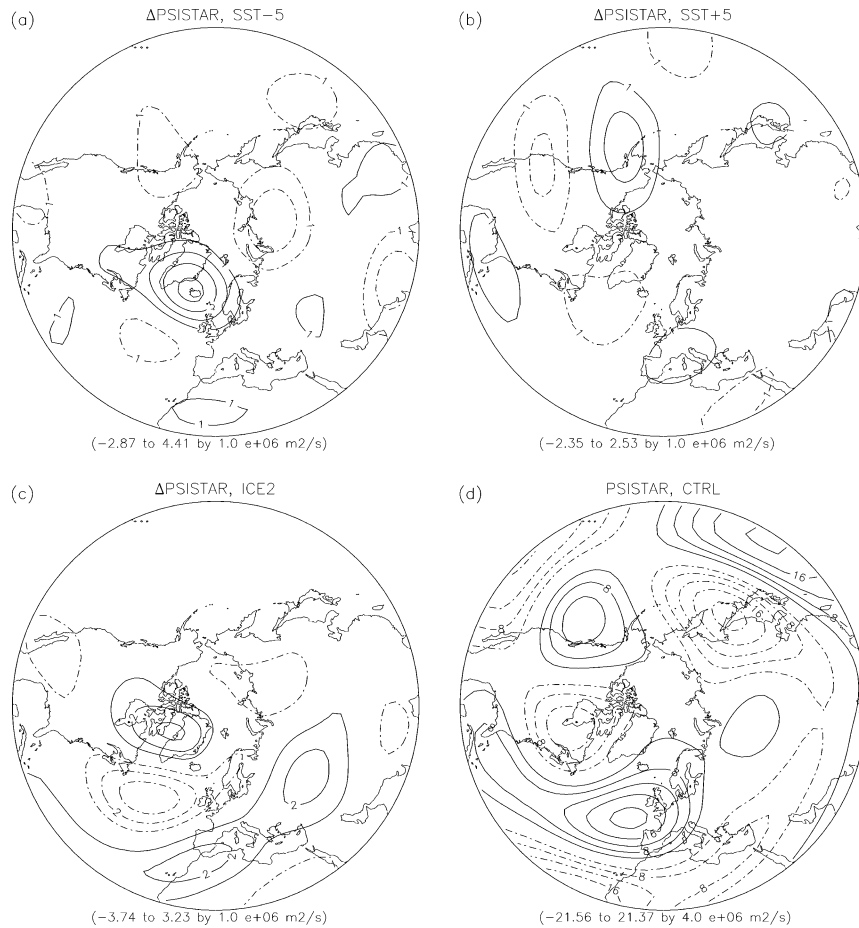


FIG. 9. DJFM-mean response in 300-hPa eddy streamfunction in $10^6 \text{ m}^2 \text{ s}^{-1}$, contour interval is 1: (a) SST-5, (b) SST+5, and (c) ICE2. Negative contours are dashed-dotted and the zero contour is suppressed. (d) DJFM-mean 300-hPa eddy streamfunction in CTRL simulation in $10^6 \text{ m}^2 \text{ s}^{-1}$ and the contour interval is 4.

four months (DJFM) of the entire time series (for each case), and the prime represents the deviation from the time mean (e.g., $x = \bar{x} + x'$). When we examine time-mean fields that are quadratic in transient eddy variables (e.g., $x'y'$), it is implicit that the fields are time filtered so that only variations of 2–8-day time scale are included.

The free tropospheric response is equivalent barotropic. Thus, there is close correspondence between the extratropical 500-hPa geopotential response seen in Fig. 3 and the 300-hPa streamfunction response (not shown). By subtracting the zonal average of the mean streamfunction response in each case, we get a representation of the stationary eddy response. Figures 9a–9c show the response in $\overline{\psi^*}$ for the different cases; Fig. 9d shows the $\overline{\psi^*}$ field for the CTRL case. Even though the free tropospheric streamfunction response is the weakest in the SST+5 case, it results in slight downstream amplification of the NA stationary waves, seen in Fig. 9b. This has important consequences for other fields in this case. The other two cases, SST-5 and ICE2, depicted

in Figs. 9a and 9c, respectively, lead to a weakened NA stationary wave pattern compared to CTRL. Both the response leading to strengthened and weakened NA stationary waves is statistically significant at 95% according to a local t test.

The response in 300-hPa zonal velocity is shown in Fig. 10. Again, the response for SST+5 (Fig. 10b) has the smallest amplitude, but it results in the downstream amplification of the NA jet over northern Europe, so that the jet (seen for the CTRL case in Fig. 10d) develops a more pronounced meridional tilt over the Atlantic in this case. Both SST-5 and ICE2 result in a jet at 300 hPa that is more zonally oriented, with reduced wind speeds on its poleward side and increased wind speeds equatorward. This and the weakened stationary waves described above are the usual accompaniment of a negative NAO scenario (e.g., DeWeaver and Nigam 2000).

The storm tracks in the CTRL case, as depicted by the high-pass-filtered 300-hPa streamfunction variance ($\overline{\psi'^2}$), are shown in Fig. 11d. The NA storm track shows

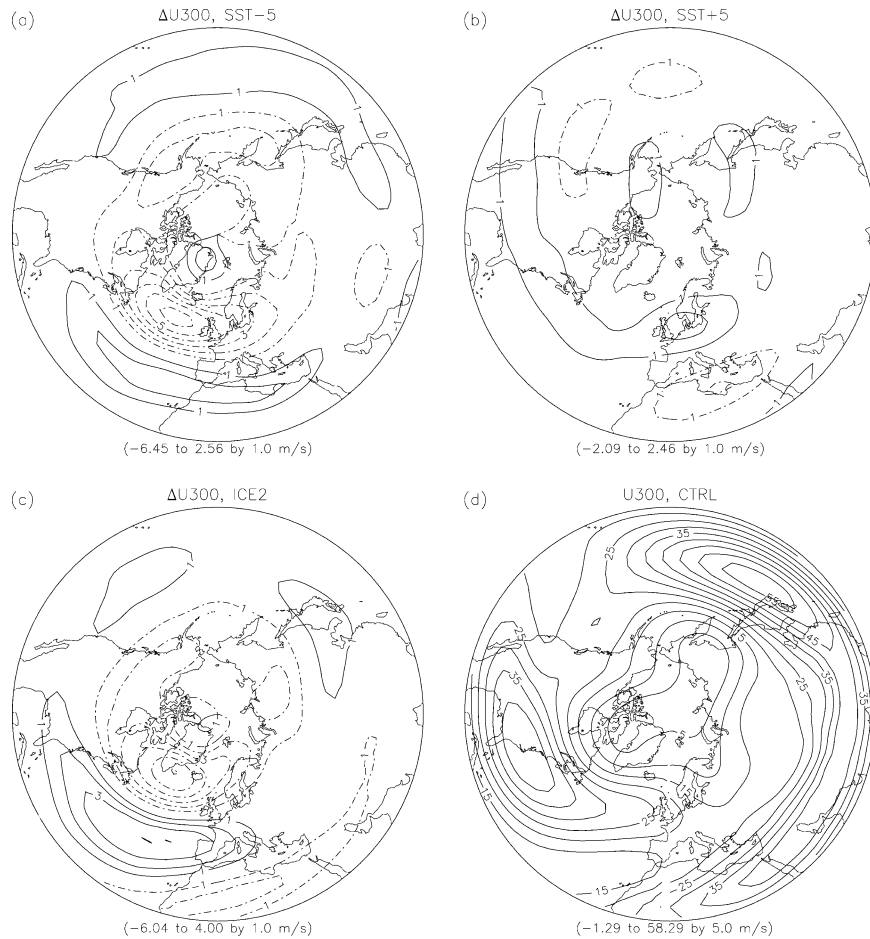


FIG. 10. DJFM-mean response in 300-hPa zonal wind in m s^{-1} , contour interval is 1: (a) SST-5, (b) SST+5, and (c) ICE2. Negative contours are dashed-dotted and the zero contour is suppressed. (d) DJFM-mean 300-hPa zonal wind in CTRL simulation in m s^{-1} and the contour interval is 5.

up as a maximum in this field stretching toward the northeast from the East Coast of the United States across the Atlantic. The response in this field for the cases SST-5, SST+5, and ICE2, are shown in Figs. 11a,b,c, respectively. Our focus here is on the region of and surrounding the NA ocean where the boundary forcing is applied. Up to this point, the response in various free tropospheric fields associated with SST-5 and ICE2 have been rather similar, especially in light of the very different boundary forcing. However, from this point on, we note several differences in the response for the two cases.

The storm track response for SST-5 (Fig. 11a) is indicative of a poleward shift in that a secondary maximum develops across Greenland around 70°N , storm activity decreases south of that latitude belt to about 40°N and then increases again, but by considerably less. This signature is robust as it shows up almost identically in both halves of the 61-yr time series. Note that in this case the decrease in storm activity is more pronounced than the increase because it reaches over a larger area. The area of increased storm activity is located over a

much narrower part of the basin. Examining the baroclinic fields to determine what supports this change in storm activity, the response in 700-hPa temperature, shown in Fig. 12a, is a warm anomaly with maximum amplitude of 4 K, on the northern side of the positive SST anomaly. The response pattern of the high-pass-filtered 700-hPa northward transient eddy heat flux $\overline{v'T'}$, shown in Fig. 13a, is such that it is negative over the area of positive SST anomaly and positive to the north, where storm track activity has increased. Thus, there is divergence of transient eddy heat flux in the area of maximum warming, which is familiar from other studies (e.g., Trenberth and Hurrell 1994; Magnusdottir 2001) and the temperature anomaly is maintained by the mean flow. A very similar signature is found for the high-pass-filtered 850-hPa northward transient eddy moisture flux. Thus, the response in the transient meridional energy fluxes supports the northward shift in storm track activity. Note that this response is at odds with the classical view of a negative NAO type response because it has been associated with a southward migration of the storm track (e.g., Wanner et al. 2001;

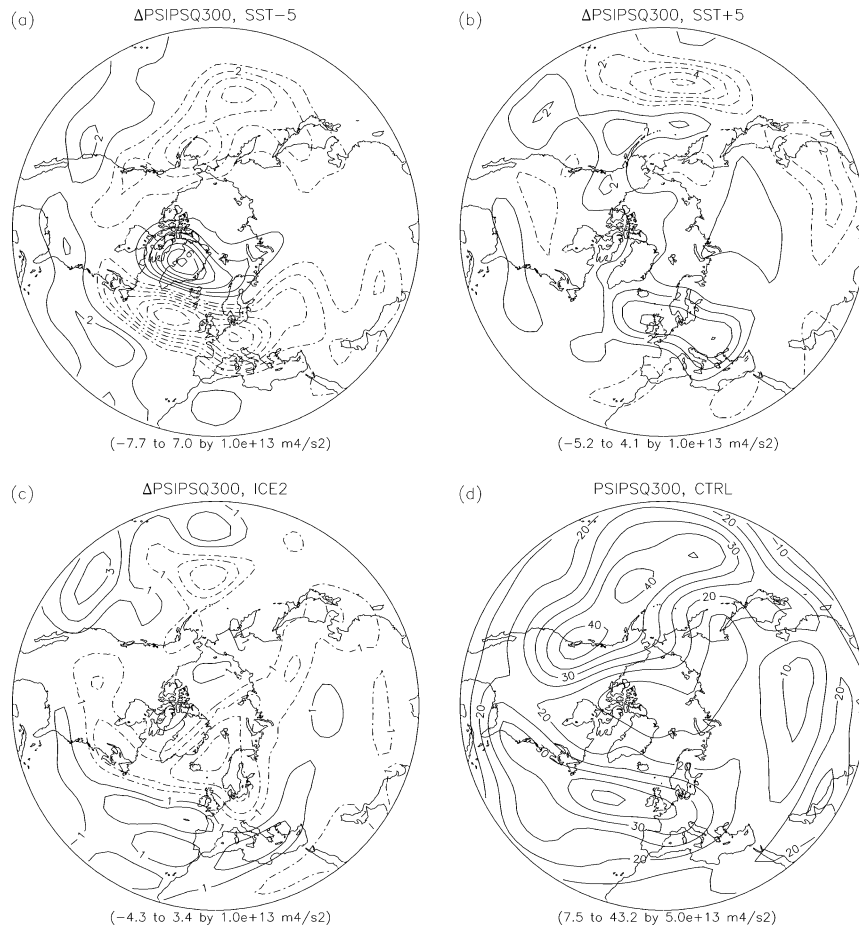


FIG. 11. DJFM-mean response in 300-hPa streamfunction variance ($\overline{\psi'^2}$) in $10^{13} \text{ m}^4 \text{ s}^{-2}$, contour interval is 1: (a) SST-5, (b) SST+5, and (c) ICE2. Negative contours are dashed-dotted and the zero contour is suppressed. (d) DJFM-mean 300-hPa streamfunction variance in CTRL simulation in $10^{13} \text{ m}^4 \text{ s}^{-2}$ and the contour interval is 5.

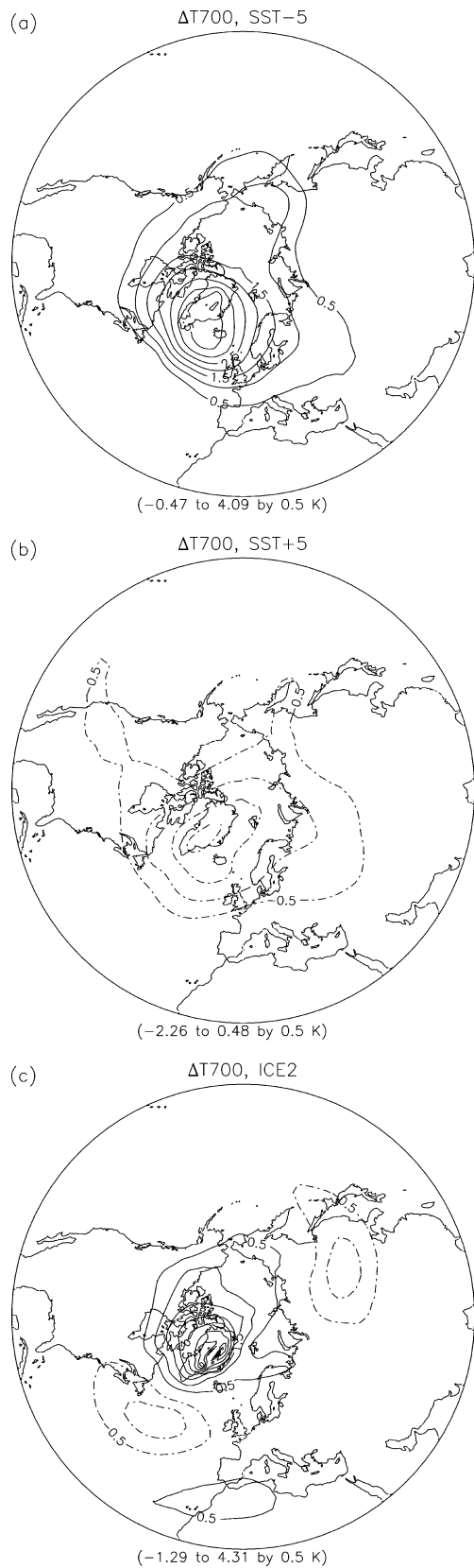
Trigo et al. 2002; Rogers 1997). However, it should be noted that the storm track as represented both by $\overline{\psi'^2}$ and $\overline{v'T'}$ is weakly amplified over the middle of the NA basin, just south of 40°N .

Let us consider the transient eddy response fields for the ICE2 case. The 300-hPa streamfunction variance, shown in Fig. 11c, depicts a general decrease in storm activity over the NA basin, north of 50°N and a smaller amplitude increase tilted northeastward over the eastern half of the basin south of about 55°N . In this case the response in 700-hPa temperature (Fig. 12c) corresponds to warming over an area that is restricted to west of the area of ice removal, immediately off the east coast of Greenland. There is an extensive area of smaller amplitude cooling south of this region, immediately south of the region where sea ice has been extended into the Labrador Sea. The 700-hPa northward transient eddy heat flux, in Fig. 13c, shows a modest increase over the southern part of the area of cooling (south of 40°N) and a much stronger decrease almost everywhere else over the NA basin. There is a small area of increased transient

eddy heat flux east of Greenland. The (co)variance fields described here are all robust, in that they are almost identical in the two halves of the entire 61-yr time series.

The picture that emerges from this simulation (ICE2) is that despite the warming of the low- to midtroposphere at high latitudes, the warming is mostly restricted to the area over Greenland and farther west. Even though there is a modest increase in transient eddy heat flux east of Greenland, it is not in an area of high baroclinity (note the small amplitude of $\overline{v'T'}$ in this area for the CTRL; Fig. 13d). One can speculate that were the continental barrier of Greenland not in the way, the eddy response might be different (see also Kristjansson and McInnes 1999). With the current land configuration, the increased baroclinity east of Greenland is simply too far removed from baroclinic energy sources for storm activity to significantly increase.

The SST+5 case turns out to be quite interesting in terms of storm track activity. Figure 11b shows the response in terms of streamfunction variance. There is increased storm track activity over the entire North At-



lantic, especially at the downstream end of the storm track, over the North Sea and northern Europe. The response in 700-hPa temperature (Fig. 12b) is cooling over the entire polar cap, note that its amplitude is less than the warming for the SST-5 case. The response in transient eddy heat flux is that of an increase right in the area of high eddy heat flux in the CTRL case, thus amplifying the storm track and leading to its downstream development. A similar signature was found in the 850-hPa transient eddy moisture flux. Furthermore, the features of the (co)variance fields described here were robust in that they were almost identical in the two halves of the 80-yr time series.

One important question that we have not addressed is how the transient eddy response in each case may be modifying the mean flow and thereby providing secondary forcing on the flow. Even though we shall not provide a quantitative answer here, by using simple arguments, we can get an indication of how the mean streamfunction may be forced by this effect. Figure 14d shows the control-case field of barotropic forcing of the mean streamfunction by the high-frequency transients. This term is the more important of two terms that appear as forcing on the streamfunction under the assumption of quasigeostrophic, inviscid flow. Hoskins et al. (1983) denoted this field by \bar{S} , where $\bar{S} = -\nabla^{-2}(\nabla \cdot \bar{\mathbf{v}}' \zeta')$ or equals the inverse Laplacian of the convergence of the transient eddy vorticity flux. As seen in Fig. 14d, this term is particularly important at the downstream end of the Pacific storm track, extending across North America, the North Atlantic, and into Eurasia. Thus \bar{S} is important in the general area of the oceanic boundary forcing. [Sections 2a,b of Magnusdottir (2001) contain more details on the physical relevance of this field as well as a comparison of \bar{S} from this control simulation (CTRL) with \bar{S} obtained from NCEP data.] Figures 14a-14c show the response in this field for the three cases, SST-5, SST+5 and ICE2, respectively. Even though the inverse Laplacian leads to spatial smoothing, admittedly the response as seen in this term is quite noisy. When we compared the two halves of the entire time series, certain features stood out and we shall concentrate on those. For SST-5 and ICE2 the response in \bar{S} corresponds to weaker flow across the North Atlantic. For SST+5, the response in \bar{S} corresponds to stronger flow over the northeastern part of the North Atlantic, close to 60°N. This is consistent with the response in mean streamfunction as well as the mean zonal flow. Thus we can infer that transient eddy feedback is important in these cases for the respective regions, even though we can only quantify this effect if we assume an upper-level barotropic flow.

FIG. 12. DJFM-mean response in 700-hPa temperature (K), contour interval is 0.5 K, and the zero contour is omitted: (a) SST-5, (b) SST+5, and (c) ICE2.

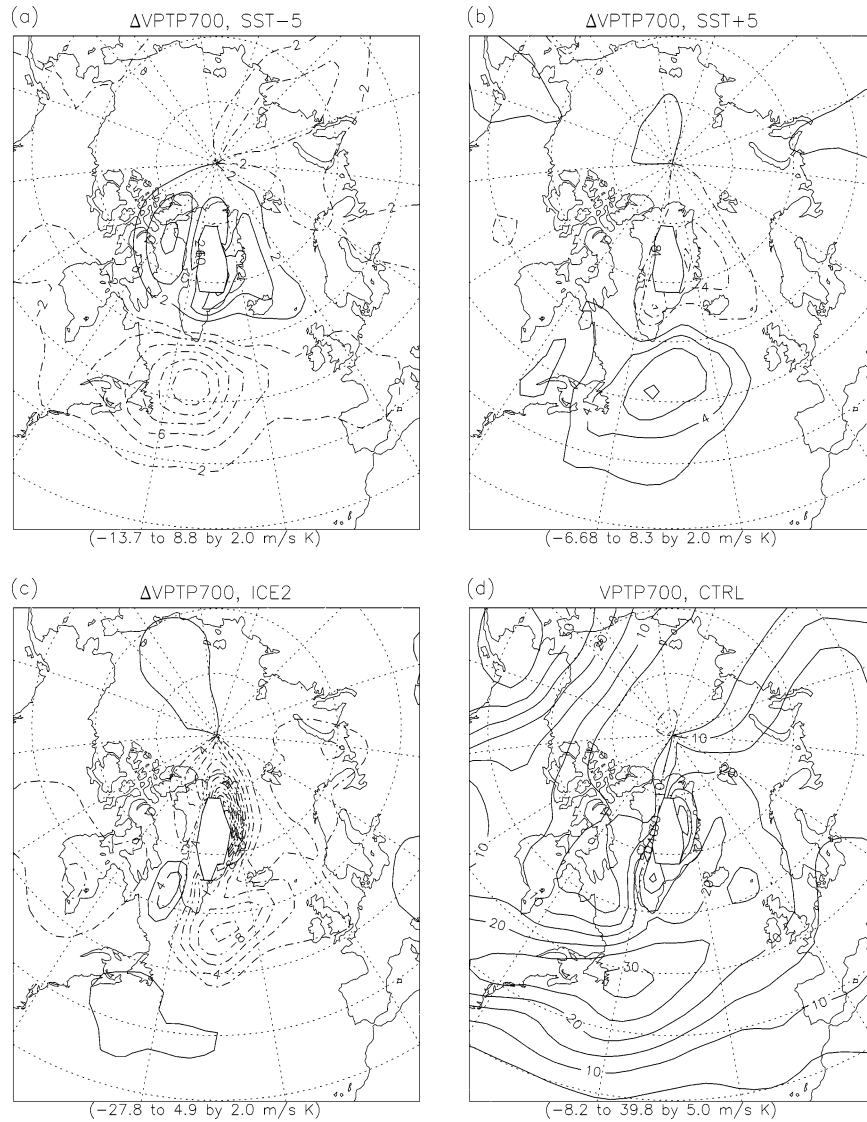


FIG. 13. DJFM-mean response in 700-hPa transient eddy meridional heat flux ($\overline{v'T'}$; in K m s^{-1}), contour interval is 2 (the projection is the same as in Figs. 1a,b): (a) SST-5, (b) SST+5, and (c) ICE2. Negative contours are dashed-dotted and the zero contour is suppressed. (d) DJFM-mean 700-hPa transient eddy heat flux in CTRL simulation (K m s^{-1}) and the contour interval is 5.

We have not attempted to provide a thoroughly comprehensive analysis of the storm track response in each case and our results are therefore not entirely conclusive. However, in light of results on the indirect (or modal) geopotential response and its deviation from the total response (the direct or nonmodal response) presented in Part II, it is interesting that the storm track response is consistent with those ideas. Thus, the two negative NAO response experiments show common elements in the storm track response, namely, a tendency for a more zonal storm track that is also detected in observations of negative NAO scenarios. This is likely associated with the indirect part of the response, whereas the many

differences between the two storm tracks are likely associated with differences between the direct (or non-modal) part of the response. The positive NAO case, SST+5, has a storm track response that is consistent with observations of the positive NAO storm track, namely, a more pronounced meridional tilt and downstream amplification. This we can likely attribute to the indirect or modal part of the response.

5. Concluding remarks

We have carried out a modeling study of the atmospheric response to oceanic boundary forcing in the

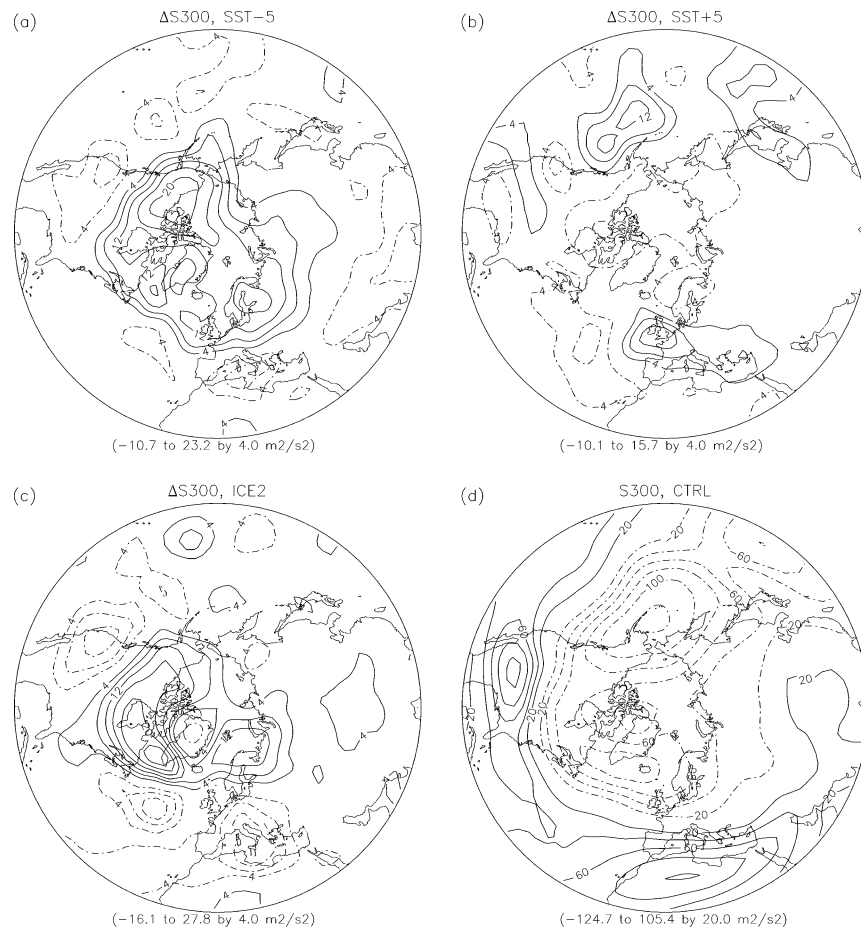


FIG. 14. DJFM-mean response in 300-hPa barotropic forcing of the mean streamfunction by transient eddies (\bar{S} ; in $\text{m}^2 \text{s}^{-2}$), contour interval is 4, negative contours are dashed-dotted, and the zero contour is suppressed: (a) SST-5, (b) SST+5, and (c) ICE2. (d) The \bar{S} for CTRL simulation in $\text{m}^2 \text{s}^{-2}$, and the contour interval is 20.

North Atlantic region. We considered two kinds of forcing: SST anomalies and sea ice anomalies. We used the observed multidecadal trends in SST and sea ice to motivate our choice for the spatial patterns of anomalous forcing, thus ensuring that our forcing has “realistic” spatial structure. However, we used exaggerated amplitudes for the strength of these anomalies to improve the signal-to-noise ratio in our numerical experiments.

We find that even with exaggerated forcing amplitudes and integrations of at least 61 yr in length, there is significant sensitivity of the response pattern to the calendar month; that is, the February response was quite different from the March response, even though the boundary forcing in each case is almost identical in winter. Only by computing wintertime seasonal averages, were we able to obtain statistically robust patterns for the atmospheric response to SST and sea ice anomalies. We expect that if we integrated longer, some of this subseasonal variability would disappear or the signal-to-noise ratio would be larger. However, some of

the variability would remain because the background flow is not the same from month to month.

Our primary finding is that the wintertime atmospheric response to the multidecadal trends in SST and sea ice resembles the NAO, to first order. However, even for the exaggerated forcing amplitudes that we have used, the atmospheric response to the SST trend pattern is quite weak compared to the observed trend in atmospheric flow. For the observed sign of the SST trend, the atmospheric response has the same sign as the observed trend. This is indicative of a weak positive feedback on the NAO, and is consistent with the SST forcing results of Rodwell et al. (1999) and Peng et al. (2002).

We find that sea ice anomalies are more efficient at exciting an atmospheric response than the SST anomalies, for the forcing amplitudes that we have considered. For the observed sign of sea ice trend, the atmospheric response has the opposite sign to the observed atmospheric trend, but is comparable in amplitude. Taking into account the factor of 2 exaggeration

in the extent of the sea ice anomaly, we conclude that the atmospheric response to the observed sea ice trend is about half the amplitude of the observed trend in 500-hPa height, but the sign of the response is opposite to the atmospheric trend, thus the feedback is negative. However, there is an important caveat. We have only considered anomalies in the extent of sea ice and not in its concentration. Other studies (e.g., Murray and Simmonds 1995; Alexander et al. 2004) have noted that changes in ice concentration (i.e., allowing for grid boxes over the ocean that are partially covered by sea ice) can also play an important role in determining the atmospheric response. Alexander et al. (2004), who used observed sea ice anomalies to force the atmosphere, reach a similar conclusion as to the sign of the feedback.

Because response to the SST anomalies is weak, we expected the overall response to the combined SST and sea ice trends to be dominated by the response to sea ice forcing. Indeed, that turns out to be the case in one additional experiment, which is forced by combining the SST anomalies corresponding to the equivalent bi-centennial trend (of SST+5) and the exaggerated sea ice anomalies (of ICE2). The response in this experiment is almost identical to that in ICE2 in all fields. This confirms our expectation that the sea ice boundary forcing in the North Atlantic sector dominates the atmospheric response and nonlinear interactions between the response to the two different types of boundary forcing are inconsequential. Since the atmospheric circulation is thought to force the observed variability in sea ice (Deser et al. 2000) as well as in SST (Seager et al. 2000) over recent decades, during which the atmospheric circulation has been characterized by a positive NAO, our modeling study suggests that the atmospheric response to observed SST and sea ice trends acts as a significant negative feedback on the whole North Atlantic climate system.

Although there are gross similarities between the atmospheric response to SST and sea ice trends and the NAO, there are also significant differences in the details. In particular, we show in Part II of this study that one can decompose the total atmospheric response into a direct response and an indirect response, with only the latter bearing a close resemblance to the NAO. Another important result that emerges from our study is that there is substantial nonlinearity in the atmospheric response to SST anomalies. Positive SST anomalies are more efficient at exciting a strong atmospheric response when compared to negative SST anomalies. This issue is also explored in more detail in Part II of the study.

We find some interesting features in the storm track response to oceanic boundary forcing. Based upon the observed relationship between the NAO and the Atlantic storm track, one would expect the positive NAO phase to be associated with a more meridionally tilted storm track. For the negative NAO phase, one would expect the storm track to be more zonally oriented. We find that the storm track response to SST and sea ice anomalies

exhibits the same sensitivities. When forced with the observed sign of the sea ice trends, the storm track tends to be more zonally oriented, corresponding to the negative NAO response. When forced with the observed sign of the SST trend, the storm track exhibits an increased meridional tilt, as expected from the weak positive NAO response. The spatial structure of the transient eddy forcing associated with the storm track response is consistent with the forcing needed to explain the tropospheric flow response, underscoring the importance of the transient eddies, as noted in other studies (e.g., Kushnir and Lau 1992; Peng and Whitaker 1999).

Although we have tried to address some of the important questions regarding the atmospheric response to SST and sea ice trends in the North Atlantic, there are still several outstanding questions. For example, we have not computed the atmospheric response to the actual trends in SST and sea ice over the last 40 years, without any exaggeration in amplitude. While this is certainly of great interest, more realistic experiments would require significantly larger computational resources so that statistically robust results may be obtained.

Acknowledgments. The authors wish to thank Xia-Lin Ma for programming support, Mike Alexander for helpful comments on the original manuscript, and three anonymous reviewers for helpful reviews. This work was supported by NOAA OGP under Grants NA96GP0420 and NA16GP2006, and NSF under Grants 9908883 and 0301800. An allocation of computer time was made by the SCD of NCAR.

REFERENCES

- Alexander, M. A., U. S. Bhatt, J. E. Walsh, M. S. Timlin, J. S. Miller, and J. D. Scott, 2004: The atmospheric response to realistic Arctic sea ice anomalies in an AGCM during winter. *J. Climate*, **17**, 890–905.
- Ambaum, M. H. P., B. J. Hoskins, and D. B. Stephenson, 2001: Arctic Oscillation or North Atlantic Oscillation? *J. Climate*, **14**, 3495–3507.
- Barsugli, J. J., and D. S. Battisti, 1998: The basic effects of atmosphere–ocean thermal coupling on midlatitude variability. *J. Atmos. Sci.*, **55**, 477–493.
- Deser, C., and M. S. Timlin, 1997: Atmosphere–ocean interaction on weekly timescales in the North Atlantic and Pacific. *J. Climate*, **10**, 393–408.
- , J. E. Walsh, and M. S. Timlin, 2000: Arctic sea ice variability in the context of recent atmospheric circulation trends. *J. Climate*, **13**, 617–633.
- , G. Magnusdottir, R. Saravanan, and A. Phillips, 2004: The effects of North Atlantic SST and sea-ice anomalies on the winter circulation in CCM3. Part II: Direct and indirect components of the response. *J. Climate*, **17**, 877–889.
- DeWeaver, E., and S. Nigam, 2000: Do stationary waves drive the zonal-mean jet anomalies of the northern winter? *J. Climate*, **13**, 2160–2176.
- Frankignoul, C., A. Czaja, and B. l’Heveder, 1998: Air–sea feedback in the North Atlantic and surface boundary conditions for ocean models. *J. Climate*, **11**, 2310–2324.
- Hack, J. J., J. T. Kiehl, and J. W. Hurrell, 1998: The hydrologic and

- thermodynamic characteristics of the NCAR CCM3. *J. Climate*, **11**, 1179–1206.
- Honda, M., K. Yamazaki, H. Nakamura, and K. Takeuchi, 1999: Dynamic and thermodynamic characteristics of atmospheric response to anomalous sea-ice extent in the Sea of Okhotsk. *J. Climate*, **12**, 3347–3358.
- Hoskins, B. J., I. N. James, and G. H. White, 1983: The shape, propagation and mean flow interactions of large scale weather systems. *J. Atmos. Sci.*, **40**, 1595–1612.
- Hurrell, J. W., 1995: Decadal trends in the North Atlantic Oscillation: Regional temperatures and precipitation. *Science*, **269**, 676–679.
- , and H. van Loon, 1997: Decadal variations in climate associated with the North Atlantic Oscillation. *Climate Change*, **36**, 301–326.
- , J. J. Hack, B. A. Boville, D. L. Williamson, and J. T. Kiehl, 1998: The dynamical simulation of the NCAR Community Climate Model Version 3 (CCM3). *J. Climate*, **11**, 1207–1236.
- Kalnay, E., and Coauthors, 1996: The NCAR/NCEP 40-Year Reanalysis Project. *Bull. Amer. Meteor. Soc.*, **77**, 437–471.
- Kiehl, J. T., J. J. Hack, G. B. Bonan, B. A. Boville, D. L. Williamson, and P. J. Rasch, 1998: The National Center for Atmospheric Research community climate model: CCM3. *J. Climate*, **11**, 1131–1149.
- Kristjansson, J. E., and H. McInnes, 1999: The impact of Greenland on cyclone evolution in the North Atlantic. *Quart. J. Roy. Meteor. Soc.*, **125**, 2819–2834.
- Kushnir, Y., and N.-C. Lau, 1992: The general circulation model response to a North Pacific SST anomaly: Dependence on time scale and pattern polarity. *J. Climate*, **5**, 271–283.
- , W. A. Robinson, I. Blade, N. M. J. Hall, S. Peng, and R. Sutton, 2002: Atmospheric GCM response to extratropical SST anomalies: Synthesis and evaluation. *J. Climate*, **15**, 2233–2256.
- Magnusdottir, G., 2001: The modeled response of the mean winter circulation to zonally averaged SST trends. *J. Climate*, **14**, 4166–4190.
- Menendez, C. G., V. Serafini, and H. Le Treut, 1999: The effect of sea-ice on the transient atmospheric eddies of the Southern Hemisphere. *Climate Dyn.*, **15**, 659–671.
- Murray, R. J., and I. Simmonds, 1995: Responses of climate and cyclones to reductions in Arctic winter sea ice. *J. Geophys. Res.*, **100**, 4791–4806.
- Peng, S., and J. S. Whitaker, 1999: Mechanisms determining the atmospheric response to midlatitude SST anomalies. *J. Climate*, **12**, 1393–1408.
- , W. A. Robinson, and S. Li, 2002: North Atlantic SST forcing of the NAO and relationships with intrinsic hemispheric variability. *Geophys. Res. Lett.*, **29**, 1276, doi:10.1029/2001GL014043.
- Rayner, N. A., C. K. Folland, D. E. Parker, and E. B. Horton, 1995: A new global sea-ice and sea surface temperature (GISST) data set for 1903–1994 for forcing climate models. Hadley Centre Internal Note 69, 9 pp. [Available from the Hadley Centre, Meteorological Office, London Road, Bracknell RG12 2SZ, United Kingdom.]
- Rodwell, M. J., D. P. Rowell, and C. K. Folland, 1999: Oceanic forcing of the wintertime North Atlantic Oscillation and European climate. *Nature*, **398**, 320–323.
- Rogers, J. C., 1997: North Atlantic storm track variability and its association to the North Atlantic Oscillation and climate variability of Northern Europe. *J. Climate*, **10**, 1635–1647.
- Saravanan, R., 1998: Atmospheric low-frequency variability and its relationship to midlatitude SST variability: Studies using the NCAR climate system model. *J. Climate*, **11**, 1386–1404.
- Schneider, E. K., L. Bengtson, and Z.-Z. Hu, 2003: Forcing of Northern Hemispheric climate trends. *J. Atmos. Sci.*, **60**, 1504–1521.
- Seager, R., Y. Kushnir, M. Visbeck, N. Naik, J. Miller, G. Krahnmann, and H. Cullen, 2000: Causes of Atlantic Ocean climate variability between 1958 and 1998. *J. Climate*, **13**, 2845–2862.
- Simmonds, I., and W. F. Budd, 1991: Sensitivity of the Southern Hemisphere circulation to leads in the Antarctic pack ice. *Quart. J. Roy. Meteor. Soc.*, **117**, 1003–1024.
- Stephenson, D. B., and V. Pavan, 2003: The North Atlantic Oscillation in coupled climate models: A CMIP1 evaluation. *Climate Dyn.*, **19**, 381–399.
- Trenberth, K. E., and J. W. Hurrell, 1994: Decadal atmosphere–ocean variations in the Pacific. *Climate Dyn.*, **9**, 303–319.
- Trigo, R. M., T. J. Osborn, and J. M. Corte-Real, 2002: The North Atlantic Oscillation influence on Europe: Climate impacts and associated physical mechanisms. *Climate Res.*, **20**, 9–17.
- Wallace, J. M., 2000: North Atlantic Oscillation annular mode: Two paradigms—One phenomenon. *Quart. J. Roy. Meteor. Soc.*, **126**, 791–805.
- Wanner, H., S. Bronnimann, C. Casty, D. Gyalistras, J. Luterbacher, C. Schmutz, D. B. Stephenson, and E. Xoplake, 2001: North Atlantic Oscillation—Concepts and studies. *Surv. Geophys.*, **22**, 321–382.